

Future possibilities of the Linac Coherent Light Source

M. Cornacchia,^{a*} J. Arthur,^a K. Bane,^a P. Bolton,^a R. Carr,^a F. J. Decker,^a P. Emma,^a J. Galayda,^a J. Hastings,^a K. Hodgson,^a Z. Huang,^a I. Lindau,^a H. D. Nuhn,^a J. M. Paterson,^a C. Pellegrini,^b S. Reiche,^b H. Schlarb,^{a‡} J. Stöhr,^a G. Stupakov,^a D. Walz^a and H. Winick^a

^aStanford Linear Accelerator Center, Stanford, CA 20450, USA, and ^bUniversity of California, Los Angeles, CA 90095, USA.
E-mail: cornacchia@slac.stanford.edu

A study of the potential for the development of the Linac Coherent Light Source (LCLS) beyond the specifications of the baseline design is presented. These future developments include delivery of X-ray pulses in the 1 fs regime, extension of the spectral range, increase of the FEL power, exploitation of the spontaneous emission, and a more flexible time structure. As this potential is exploited, the LCLS can maintain its role as a world-leading instrument for many years beyond its commissioning in 2008 and initial operation as the world's first X-ray free-electron laser.

Keywords: free-electron lasers; Linac Coherent Light Source.

1. Introduction

This report addresses the potential for the development of the Linac Coherent Light Source (LCLS) at the Stanford Linear Accelerator Center (SLAC) beyond the performance anticipated in the baseline configuration which is expected to start operation in September 2008. This facility (LCLS, 2002), a linac-based free-electron laser (FEL) based on the self-amplified spontaneous-emission (SASE) process operating in the X-ray region of the spectrum, is scheduled to start operation with extraordinary peak brightness, flux, coherence and ultrashort subpicosecond pulses. The further developments discussed in this paper concern the following characteristics: (i) femtosecond (fs) pulses (§2); (ii) expanded photon energy range (§§3.3 and 3.4); (iii) increased FEL power (§§3.1 and 5.1); (iv) characteristics and applications of the spontaneous radiation (§4); (v) flexibility in pulse timing structure (§5.2). Table 1 presents a list of the most important performance parameters of the LCLS as specified in the *LCLS Conceptual Design Report*, henceforth referred to as 'baseline LCLS' (LCLS, 2002), together with the potential for expansion of the same parameters that will be possible with the upgrades described in this paper.

Some of the upgrades, such as a reduction of FEL pulse length, will be studied soon after the LCLS is commissioned. Others, like the expanded range of the photon energy and the pulse timing structure, will require more involved modifications that will build on the investment already made. This report does not discuss the use of multiple undulators§ into which the photon beam is switched to provide for several simultaneous users: this is considered to be a conceptually straightforward extension that will be part of the natural development of the LCLS in the early years of operation. The

‡ On leave from Deutsches Elektronen-Synchrotron DESY, D-22603 Hamburg, Germany.

§ In this report the term undulator is loosely used to indicate both a wiggler and an undulator.

Table 1

FEL parameters of the LCLS in the baseline design and in the upgrade.

	Baseline LCLS	Upgraded LCLS
Spectral range (nm)/(keV)	0.15–1.5/8.3–0.83	0.012–5/100–0.25
Peak FEL power (GW)	8–19	Up to 200
Number of FEL pulses per macropulse	1	1–60, flexible
Pulse duration FWHM (fs)	<230	<1

upgrades proposed in this paper could take place during the first ten years of the LCLS operation.

2. Femtosecond pulses from the LCLS

2.1. General introduction and review of methods to shorten the FEL pulse length

The basic time structure of a SASE FEL is determined by the electron pulse time structure, the undulator length, the cooperation length, the correlated frequency distribution obtained by chirping the electron energy distribution, and by the optical instrumentation used to shape the pulse.

2.1.1. How FEL physics determines the bunch length. A single electron moving along an undulator produces a wave train with a number of waves equal to the number of undulator periods, N_U ; if λ is the radiation wavelength, the pulse length is λN_U , the pulse duration is $\lambda N_U/c$ (c = speed of light in a vacuum), and the relative line width is $\Delta\omega/\omega = 1/N_U$. The FEL amplification process, with a gain length L_G , establishes a correlation between electrons within a cooperation length $L_C \simeq (\lambda/\lambda_U)L_G$, where λ_U is the undulator period and L_G is the field gain length; the result is that the output of a SASE-FEL consists of a series of spikes, of random amplitude and separated by a distance $2\pi L_C$. In the baseline LCLS the time duration of the electron bunch is about 230 fs (full width at half-maximum, FWHM) and $N_U \simeq 3300$, giving for the fundamental line width $\Delta\omega/\omega = 5 \times 10^{-4}$. At 1.5 Å the cooperation length is $L_C \simeq 50$ nm, and the separation between spikes is about 1 fs. The FWHM duration of a spike is about $2.3 \times L_C/c$, or about 300 attoseconds. This is the shortest conceptual pulse length that can be obtained at the LCLS. The total number of spikes is about 250 per pulse. Note that the electron beam quality plays a role in determining the ultimate limit of the FEL pulse length, *i.e.* the limit on the length of a spike: an improved beam quality, as for instance a smaller emittance or a larger peak current, reduces the gain length and the cooperation length, and thus also the spike length, with the potential of moving X-ray FEL pulses further into the attosecond region. For a more detailed description of the FEL physics see, amongst others, Bonifacio *et al.* (1984), Kim (1986), Yu *et al.* (1990), Wang & Yu (1986), Moore (1985), Scharlemann *et al.* (1985) and Xie & Deacon (1986).

2.1.2. Overview of methods to shorten the pulse length. Several authors have discussed methods of reducing the X-ray pulse length of the LCLS below the baseline value of 230 fs (*e.g.* Bharadwaj *et al.*, 2000). These reports discuss the production of short X-ray pulses by several methods: enhanced electron bunch compression; electron bunch and X-ray energy chirping; use of optical instruments to select a part of the pulse; use of wake fields or other means to degrade the electron beam quality to prevent lasing for a large part of the electron bunch while preserving it in a small part. An overview of the results of these studies is shown in Table 2.

(i) Table 2 shows that, by using additional electron beam compression, Case *B*, it is possible to reach the 100 fs region without loss of photons per pulse.

Table 2

Comparison of X-ray pulse characteristics for eight cases at a wavelength of 1.5 Å.

Case A: LCLS baseline case. Case B: with additional electron bunch compression. Case C: spatially chirped electron beam. Case D: with chirped electron beam and pulse slicing at the undulator exit. Case E: with two-undulator system. Case F: with undulator wake fields. Case G: slotted-beam spoiler. Case H: slotted-beam spoiler with stronger compression. The last two cases (G and H) are new concepts and are described in more detail in the latter part of §2.2). A similar trend is expected at longer wavelengths, although the actual numbers may be different, reflecting different optical systems.

	Pulse duration FWHM (fs)	Electron beam energy chirping (%)	Number of photons per pulse ($\times 10^{12}$)	SASE intensity fluctuations (%)	Relative line width (%)	Central wavelength fluctuations (%)
Case A	230	0	1	7	0.1	0.2
Case B	<100	0.5	1	10	1	0.2
Case C	30	0	0.1	22	0.1	0.2
Case D	15	1	0.02	14	0.07	0
Case E	30	1	0.1	18	0.07	0
Case F	5	0	0.03	40	0.1	0.2
Case G new	4	0	0.02	40	0.1	0.2
Case H new	<1	0	0.005	50	0.1	0.2

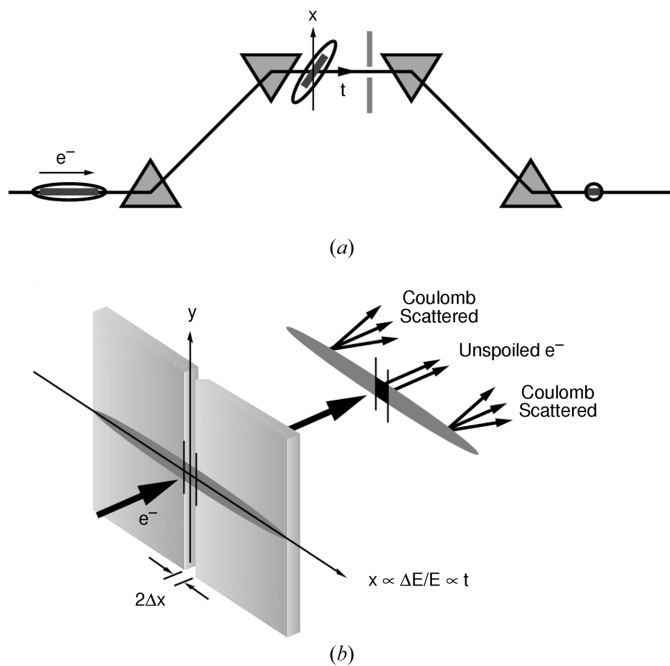


Figure 1 (a) Sketch of the electron bunch at the center of the compressor chicane with tilted beam in the horizontal direction, x , and time, t . (b) The slotted foil at the chicane center leaves a narrow unspoiled beam center.

- (ii) Using electron energy chirping and optical elements to select a short pulse at the undulator exit, Case D, it is possible to reach the 15 fs region with some loss in the number of photons per pulse.
- (iii) The two-undulator scheme, Case E, can produce 30 fs-long pulses with a reduction in the number of photons per pulse.
- (iv) By using the undulator vacuum pipe wake fields with enhanced resistivity, Case F, it might be possible to reach even a shorter pulse length, about 5 fs, with very large peak power,† about 10 GW, with little or no loss in intensity. This option requires replacing the copper-plated baseline LCLS vacuum chamber with one of high resistivity.

† Unless denoted otherwise, in this report the peak power, or just power, is the power averaged over the duration of the FEL pulse.

(v) In case C the electron bunches are given a spatial chirp instead of an energy chirp. The spatial chirp is a transverse offset (in horizontal or vertical phase spaces) correlated with the longitudinal bunch position and may be produced, for example, by a transverse deflecting cavity. Since the FEL gain is very sensitive to any initial offset in the transverse phase space at the entrance of the undulator, only a small portion of each electron bunch with relatively small transverse offsets will interact significantly with the radiation, resulting in an X-ray pulse length much shorter than the total length of the electron bunch. An initial study suggests that a 30 fs X-ray pulse length may be generated using this method.

(vi) Case G is also based on spoiling the beam phase space density in part of the electron bunch so that that part will not lase, while preserving lasing in a short length of the bunch. The proposal is to use a slotted thin foil, in a chicane section of the linear accelerator, to scatter the electrons and blow up the emittance except in a short length of the bunch. This scheme is discussed separately in the following section.

(vii) In Case H the principle is the same as that in Case G, except that the increased compression allows for a narrower slit and an electron pulse through it that is 2 fs long, generating a gain-narrowed FEL pulse that is shorter than 1 fs.

2.2. A novel way to generate femtosecond pulses: the slotted spoiler method

One promising method (Emma *et al.*, 2004) is to place a very thin beam-intercepting foil in the center of a bunch compressor chicane. The foil includes a vertically oriented narrow slot at its center and therefore spoils the horizontal and vertical emittance of most of the beam, but leaves a very thin unspoiled beam center (see Fig. 1). The following subsection examines the dynamics of the electron bunch through the foil, and also shows that the FEL pulse will be even shorter than the length of the electron bunch.

2.2.1. Generating a few femtosecond-long electron pulse.

Since the horizontal position, x , of the particles in the chicane situated at the 4.54 GeV energy point in the baseline LCLS design is highly correlated with the time of arrival of the electrons in the bunch, t (see Fig. 2), after the chicane the unspoiled beam center will become a very short duration unspoiled section of the electron bunch. The remainder of the bunch will have its emittance increased by a factor of about five (depending on foil thickness and material) through coulomb scattering, suppressing the FEL gain of those sections, but allowing nominal FEL gain for the unspoiled center of the bunch. The advantage of this differential spoiling scheme over particle collimation is that the entire electron bunch is allowed to propagate and accelerate down the linac, allowing normal function of beam diagnostics (*e.g.* beam position monitors *etc.*) and stabilization of the energy and trajectory with feedback systems. Collimation to less than 10 fs would leave only 5% of the bunch charge (<50 pC), which would be difficult to diagnose and stabilize. In addition, the wake fields of a thin foil are expected to be much less severe than those of a long dense collimator.

The ultimate limit to pulse shortening using this technique is the betatron beam size in the spoiler. The total r.m.s. beam size, σ_x , in the chicane center has contributions from both the betatron beam size, $(\beta_x \epsilon_x)^{1/2}$, and the dispersed correlated energy spread, $\eta_x \sigma_\delta$, of the beam,

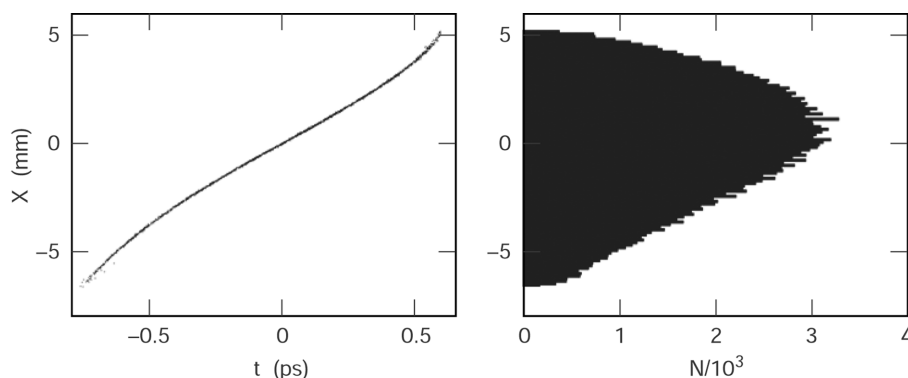


Figure 2
Distribution of electrons at the chicane center showing the very strong position–time (x – t) correlation (tilt).

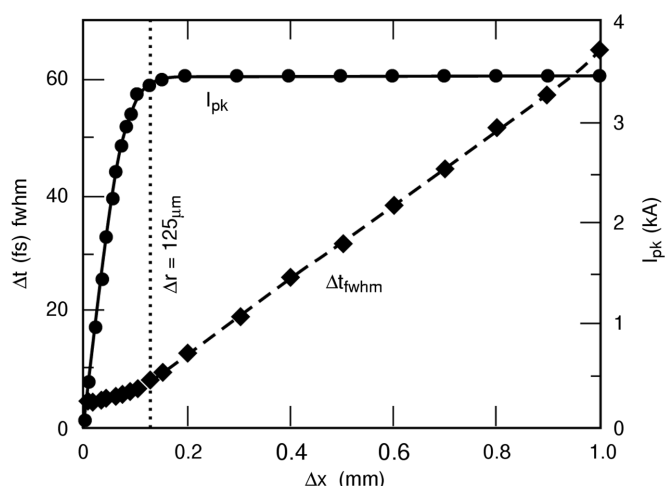


Figure 3
Peak current (circles) and FWHM pulse length (diamonds) of unspoiled electrons versus slot half-width. The minimum electron pulse length at full current is 8 fs with a 0.125 mm slot half-width.

$$\sigma_x = (\beta_x \varepsilon_x + \eta_x^2 \sigma_s^2)^{1/2}. \quad (1)$$

If the slit full-width, $2\Delta x$, is set to a few times the r.m.s. betatron beam size (*i.e.* $2\Delta x \simeq 5(\beta_x \varepsilon_x)^{1/2}$, but the foil width covers the entire beam size, $\sigma_x \gg (\beta_x \varepsilon_x)^{1/2}$, the final peak current of this slice is maintained and the nominal FEL gain applies to this very narrow beam section. The baseline LCLS second bunch compressor, BC2, has a betatron beam size $(\beta_x \varepsilon_x)^{1/2} \simeq 50 \mu\text{m}$, but a full beam size $\sigma_x \simeq 2.6 \text{ mm}$, so that a slit full-width of $\Delta x = 125 \mu\text{m}$ would produce an unspoiled bunch length section of $\sim 8 \text{ fs}$ FWHM after the chicane (Fig. 3). A smaller slit width can be used to produce a shorter pulse length, but at $\Delta x < 125 \mu\text{m}$ the peak current begins to drop and this shorter pulse will not saturate the FEL.

After the chicane the spoiled part of the beam is smeared in z enough to also overlap the unspoiled part, resulting in an increased peak current over this short duration of the beam. The FEL gain, however, will still apply to the unspoiled beam and is not affected by overlap of the spoiled beam. Inevitable energy variations (jitter) of the incident electron bunch at the foil translate into horizontal position jitter at the foil. The expected level of 0.1% energy jitter translates into 0.3 mm of horizontal jitter. Since the horizontal (and temporal) bunch distribution is fairly flat over small margins (Fig. 2), these energy variations create very little charge jitter ($\sim 2\%$) if the foil slot is initially well centered on the bunch. Since the foil slot is fixed in its horizontal position, the energy is also fixed through the slit

and the z -energy correlation translates the energy deviation into bunch arrival time jitter. In this case, a 0.1% energy jitter becomes an 80 fs timing jitter.

The system offers simplicity and flexibility. The foil slot width might also be tapered, so that varying the vertical displacement of the foil allows the selection of a different X-ray pulse length. A slot-width variation from 0.25 mm up to 2 mm allows any unspoiled electron pulse length from 8 fs all the way up to 100 fs; and, of course, removal of the foil still allows the nominal LCLS pulse length of 230 fs with the full photon flux. Finally, double-slotted foils

might allow the generation of two very short consecutive pulses which are well separated in time based simply on the physical slot separation. Tracking studies have been used to evaluate the performance of the slotted spoiler. The coulomb scattering of an electron bunch passing through a 20 μm -thick beryllium foil was simulated using the code *Elegant* (Borland *et al.*, 2002). The computation goes beyond the standard Moliere formula used in Monte Carlo simulations (see <http://pdg.lbl.gov>, p.184) and includes the case of a very thin foil of thickness $\Delta z < 10^{-3} X_0$, where X_0 is the radiation length of the material ($X_0 = 400 \text{ mm}$ for beryllium) and $\Delta z = 20 \mu\text{m}$. Figs. 4 and 5 show the r.m.s. angular divergence in x and y ($\beta_{x,y} = 25 \text{ m}$, $\gamma \varepsilon_{x,y} = 1 \mu\text{m}$, $\gamma mc^2 = 4.54 \text{ GeV}$) before and after the foil. Even with a very thin foil where $z/X_0 \simeq 5 \times 10^{-5}$, the core of the beam is scattered enough to increase the divergence by a factor of $x'/x'_0 \simeq 5$, resulting in a relative emittance growth in x and y of $\varepsilon/\varepsilon_0 \simeq [1 + (x'/x'_0)^2]^{1/2}$. A few particles are scattered out to large angles, creating tails (not shown in the figure), but their number is very small (0.3% of the population at amplitudes larger than $10\sigma_x$).

Tracking studies have also been carried out to include a 250 μm slit in a foil, where the electron bunch is tracked all the way from the photoinjector, through the slotted foil and the linac to the start of the undulator, where the electron energy is 14.3 GeV. The full longitudinal distribution of all particles is shown in Fig. 6, where a sharp spike at the bunch center appears owing the local ‘hot spot’ created by the slot in the foil. The r.m.s. temporal smearing, $\Delta\sigma_t$, is given by the r.m.s. coulomb scattering angle of the foil, θ_{rms} , times the peak dispersion in the chicane ($R_{52} = -\eta_x$), or $\Delta\sigma_t \simeq |\eta_x| \theta_{\text{rms}}/c$ which is $(320 \text{ mm})(10 \mu\text{rad})/(3 \times 10^8 \text{ m s}^{-1}) \simeq 10 \text{ fs}$. The desire to keep the final bunch length, 75 fs r.m.s., through the linac almost unchanged in order to keep the linac wake fields unchanged limits the amount of scattering (or foil thickness) that can be used to approximately the 25 μrad level (*e.g.* a 50 μm -thick beryllium foil).

The final temporal distribution of the unspoiled electrons (now starting from an idealized Gaussian bunch in this case) is shown in Fig. 7. The FWHM length of the unspoiled electron pulse length is 8 fs and the final X-ray pulse after SASE saturation is even shorter than this, as shown in the next subsection.

2.2.2. FEL gain of spoiled and unspoiled beams. It was discussed in the previous section that some spoiled electrons will be smeared in time to overlap the unspoiled electrons, resulting in an increased peak current and also a larger r.m.s. emittance for the whole beam in the 8 fs time window. The spoiled beam has transverse emittances that are about a factor of five (in each transverse dimension) higher than those of the beam that goes through the slot and, for this reason, the spoiled electrons do not affect the FEL process of the unspoiled electrons. The effect of this ‘halo’ beam was studied by considering a coasting beam with two Gaussian distributions in the transverse

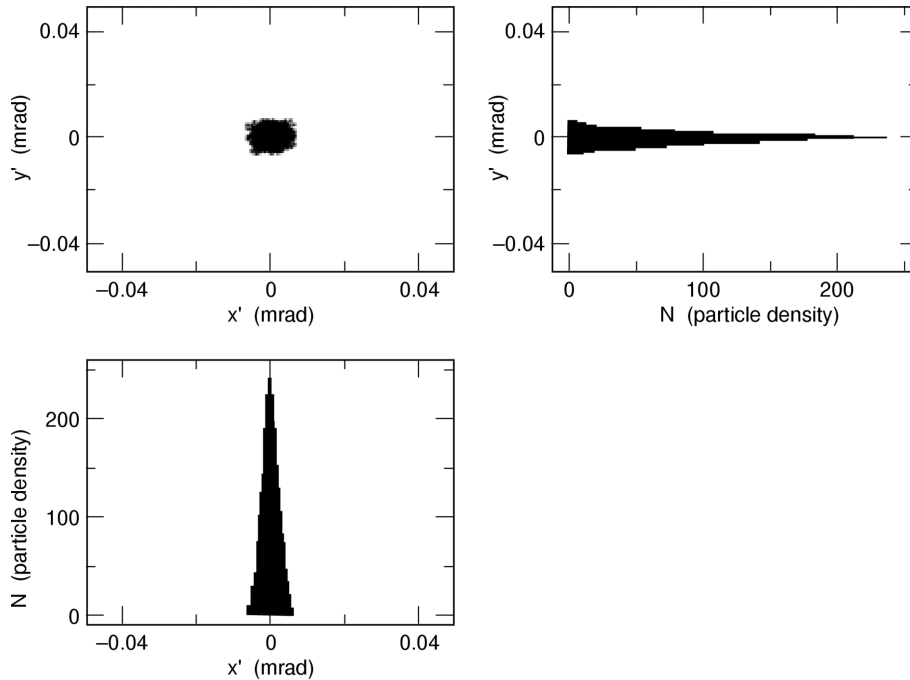


Figure 4
Beam angular divergence immediately before the foil with an r.m.s. size of 2.2 μrad .

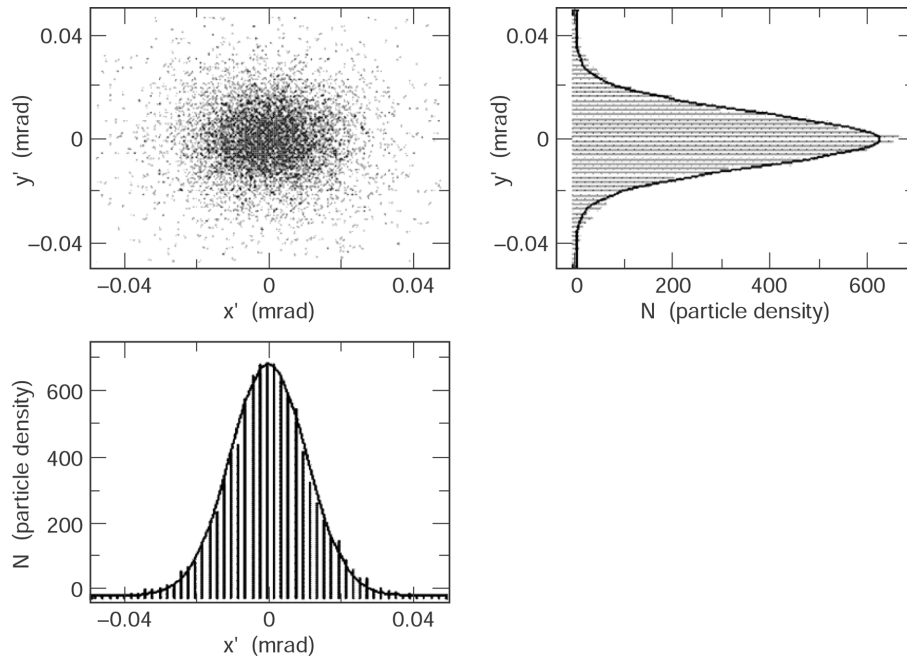


Figure 5
Beam angular divergence immediately after the foil with an r.m.s. size of 10.4 μrad .

phase space (x, x', y, y') , each representing the unspoiled and the spoiled beams. A peak current of 3 kA, 0.9 μm normalized emittances in both the x and y directions, and 0.01% r.m.s. energy spread at 14.3 GeV were assumed for the unspoiled beam. For the spoiled beam, the peak current was 2 kA, the normalized emittances were 5.4 μm in each plane, and the r.m.s. energy spread was 0.03%. Using a variational method to solve the three-dimensional FEL dispersion relation (Yu *et al.*, 1990; Xie, 2000) a power gain length of 3.74 m for a double-Gaussian distribution was found, which is very close to the

power gain length of 3.73 m of the unspoiled beam alone. Thus, the spoiled beam does not contribute to the FEL gain of the unspoiled beam. It will contribute, however, to the background of the spontaneous emission. Fig. 7 shows that the time distribution of the unspoiled beam is almost Gaussian; since the slippage length of the FEL (of the order of 1 fs) is much smaller than the FWHM length of the pulse, we may assume that the gain process is localized and determined only by the local current. The latter can be approximated by the expression of a Gaussian distribution,

$$I(t) = I_0 \exp(-t^2/2\sigma_t^2). \quad (2)$$

In the exponential gain regime the radiation generated by the highest local current grows the fastest. As a result, the length of the X-ray pulse is 'gain-narrowed' compared with the bunch length of the unspoiled beam. To estimate this gain-narrowing effect, we apply the one-dimensional FEL theory to write

$$L_G(t) = L_{G0} [I_0/I(t)]^{1/3}, \quad (3)$$

where L_{G0} is the power gain length corresponding to the peak current I_0 . The SASE power evolves as $\sigma_{ix} = \sigma_t(3L_{G0}/z)^{1/2}$, where L_{G0} is the r.m.s. X-ray pulse duration. At saturation $z = 20L_{G0}$, yielding $\sigma_{ix} = 0.4\sigma_t$. Thus, the unspoiled beam section of length 7.5 fs (FWHM) generates roughly 3 fs (FWHM) X-rays at saturation. *This bunch length reduction factor, 2.6, applies to any distribution of charge Gaussian in time at the onset of saturation.* After saturation, the unsaturated X-ray pulses (at lower local current) will continue to grow, and the pulse length will increase relative to the minimum X-ray pulse length at saturation. The FEL performance of this beam was computed using the time-dependent *GENESIS* (Reiche *et al.*, 2002) simulation that takes into account the radiation slippage. Fig. 8 shows a 2–3 fs FWHM FEL X-ray pulse at saturation ($z \simeq 60$ m) along with the 200 fs-long electron current pulse. The almost imperceptible baseline power is dominated by the spontaneous undulator radiation emitted from the 200 fs-long electron bunch.

It has been shown so far that it is possible and practical to produce X-ray pulses with a duration of ~ 3 fs FWHM. Now it will be shown that, by changing the electron compression parameters, it is possible to further reduce the FEL pulse length to the level of 1 fs or less. As the electron bunch becomes shorter and approaches the slippage length, the method used in the previous subsection is no longer applicable and a full simulation of the FEL process is required, and this is what has been done. If the electron bunch is compressed in the BC2 chicane to 10 μm r.m.s. (rather than the 22 μm of the baseline

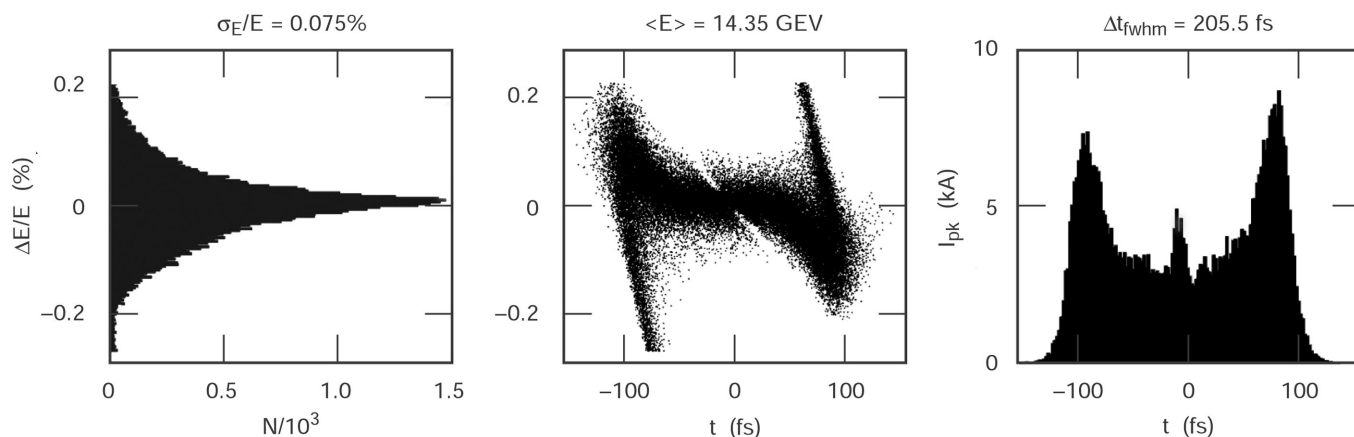


Figure 6 Longitudinal phase space at the undulator entrance (14.3 GeV) when a thin slotted-spoiler foil is placed at the center of the BC2 chicane. The central spike contains the peak current of the beam that passes through the slit plus the time-smeared electrons near but outside the slit.

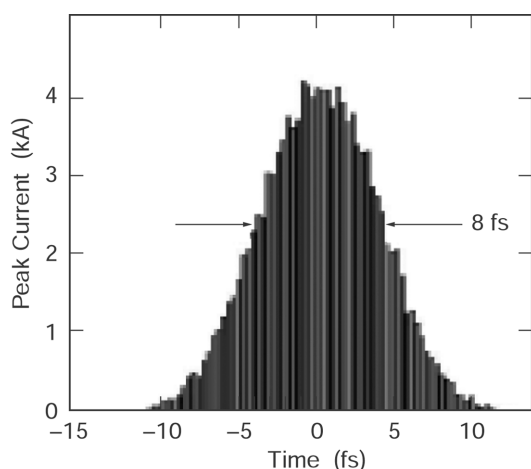


Figure 7 Unspoiled electron beam length after a thin slotted-spoiler foil at the center of the BC2 chicane.

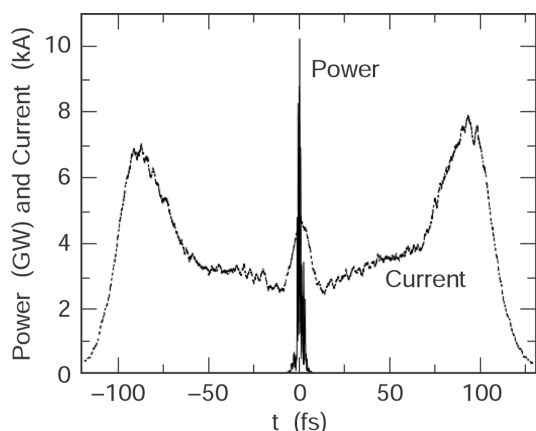


Figure 8 Electron current and *GENESIS* simulation of a 2–3 fs FWHM X-ray pulse at saturation.

LCLS) by shifting the pre-BC2 linac RF phase farther off crest by 1.6° , the peak current at the bunch center increases from 3.4 to 7.5 kA. This allows the slot width to be decreased even further until the unspoiled peak current is again lowered to 3.4 kA. The smaller

slot width, $2\Delta x = 75 \mu\text{m}$, produces a shorter unspoiled electron bunch. In addition, at this very narrow slot width, the intrinsic (uncorrelated) energy spread of the bunch needs to be $< 6 \times 10^{-6}$ r.m.s. This is achievable, since the full simulations of the LCLS, which include space-charge forces in the injector and synchrotron radiation in the linac bending systems, predict an intrinsic energy spread of $< 3 \times 10^{-6}$ at 4.54 GeV. The electron bunch length with the additional compression is 2 fs FWHM (or about 0.8 fs r.m.s.). This length is comparable with the total FEL slippage length. Near the FEL saturation (after about 70 m of undulator), the X-ray pulse length is gain-narrowed to 0.36 fs r.m.s. (~ 1 fs FWHM); this number is close to the prediction of the steady-state one-dimensional theory. Thus, the minimum FWHM X-ray pulse length generated by such a short electron beam is predicted to be below 1 fs.

3. Extension of output power and spectral range

This section explores ways in which the output power of the FEL radiation can be increased well beyond the LCLS baseline design and discusses the potential for extending the wavelength range accessible to the LCLS. It will be shown that the flexibility of the 50 GeV SLAC linac allows a considerable expansion in reachable FEL photon energies, both in the direction of shorter and longer wavelengths.

3.1. Increase of output power

The power level at saturation is determined by the q parameter (Bonifacio *et al.*, 1984)

$$P_{\text{sat}} = qP_{\text{beam}} \quad (4)$$

where

$$P_{\text{beam}} = I_p \gamma mc^2 / e \quad (5)$$

is the beam power, I_p is the peak current, γmc^2 is the electron energy and e is the electron charge. It appears more judicious to try to increase the saturation power with a larger beam current and/or q parameter, although the control on these quantities is limited. Actually, the most promising way to achieve the goal is the method of tapering the magnetic field of the undulator (Fawley *et al.*, 2002).

3.2. Increasing the power output by undulator field tapering

The concept of undulator tapering starts from the well known fundamental formula linking the radiation wavelength to the magnetic field of the undulator,

$$\lambda = [\lambda_u(z)/2\gamma(z)^2][1 + a_u(z)^2]. \quad (6)$$

Tapering consists of slowly reducing the field strength of the undulator field, contained in $a_u(z)$, to preserve the resonant wavelength λ as the energy γ changes (Scharlemann, 1990). Fig. 9 shows the performance of tapered and untapered undulators at the LCLS at 1.5 Å. It also indicates that a further increase in power is achievable by starting the FEL process from a ‘seed’ radiation (FEL amplifier) rather than from noise. This is due to the fact that in the SASE regime the light continues to grow (albeit at a reduced rate) in the saturation regime, thus reducing the benefit of tapering. The other reason is the higher degree of coherence of the radiation in the seeded case, thus involving, with tapering, a larger portion of the bunch in the energy–wavelength synchronism.

In any case, the gain from tapering the undulator is considerable. At the baseline undulator length, 120 m, the FEL output is enhanced by a factor of three, from 20 to 60 GW, with a taper of 0.4% of the undulator parameter over the last 30 m after saturation. With the present baseline design this option would require a modification of the last 30 m of the undulator. Ultimately, a 200 m tapered undulator with seeded radiation would be able to deliver output power approaching 200 GW with a taper of 1% over the last 130 m. This upgrade would require a modification to the geometry of the undulator location to direct the radiation into the far hall. The beginning of tapering has to match the saturation point; since both upgrades would take place after the saturation point along the undulator length has been experimentally determined, the taper could be defined in advance without the need of a variable-gap undulator. Given the dependence of the saturation length on the quality of the electron source, however, and given that the latter might improve in time, a variable-gap undulator would be preferable.

3.3. Operation at longer wavelengths

The baseline specifications of the LCLS give a range of wavelengths between 15 and 1.5 Å, corresponding to an energy range of the electron beam between 4.5 and 14.5 GeV. The last bunch compressor of the beamline operates at 4.5 GeV: without further acceleration, this beam would lase at a radiation wavelength of 15 Å with the baseline LCLS undulator. As the ρ parameter increases at lower beam energies, there is no limit in principle on the longest achievable wavelength because the saturation length stays shorter than 100 m. The extension of the wavelength range to 50 Å would cover the water window in the VUV region, opening the facility to a

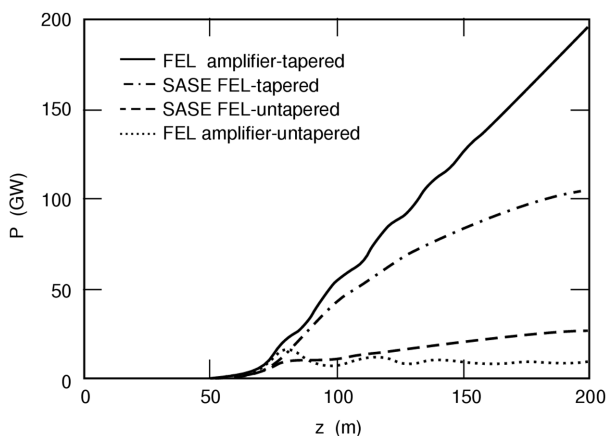


Figure 9 Radiation power versus position along the undulator for a tapered and untapered undulator field at 1.5 Å.

new class of experiments. This study will consider two possibilities: the first is to keep the undulator parameters the same as those of the baseline design and just lower the electron energy and the focusing quadrupoles; the second option holds the energy at the baseline value (14.5 GeV) and chooses the undulator period length to match the 50 Å wavelength.

3.3.1. Operation at 50 Å with the baseline undulator. With the baseline undulator parameters, the electron energy to generate 50 Å radiation is 2.5 GeV. One practical limit to long wavelengths is that the electron optics of the undulator in the baseline LCLS design cannot confine a beam with energy below 3 GeV. The 2.5 GeV beam would be overfocused and lost after a few cells of the focusing optics. Thus, in order to reach 50 Å, it would be necessary to alter the electron optics in the undulator. This could be done by reducing the quadrupole field strength, either by replacing the presently envisaged set of permanent magnets or by lowering the focusing strength in ways that it does not appreciably affect the baseline LCLS. Without any change to the baseline LCLS undulator, the lowest reachable photon wavelength is about 35 Å. In Fig. 10 the evolution of the radiation power at a wavelength of 50 Å is shown.

The electron energy is 2.5 GeV and the field strength of the LCLS quadrupoles is lowered by 40% compared with the 1.5 Å case. The FEL saturates within 10% of the total undulator length, including degrading effects such as undulator wake fields and mismatch of the individual slices of the electron beam. The resulting minimum and maximum values of the β -function are 2 m and 12 m, respectively. The simulation is ‘start-to-end’, i.e. it includes the tracking of the electron beam in the linac using the code *Elegant* (Borland *et al.*, 2002) as well as the FEL simulation with wake fields in the undulator (Reiche *et al.*, 2002). The beam is decelerated after the second bunch compressor to keep the compressor settings constant.

3.3.2. Operation at 50 Å with a dedicated undulator and comparison with the baseline undulator parameters. If the electron energy is that of the upper limit of the range of the baseline design (14.3 GeV) the undulator period length increases, for a resonant wavelength of 50 Å, from 3 to 8 cm. A not-yet optimized design of the undulator parameters produced, when computed with the code *GENESIS*, an FEL pulse of 100 GW in a 70 m-long undulator. The build-up of the power along the undulator is shown in Fig. 11.

Table 3 indicates the choice between a baseline undulator applied to 50 Å with an electron energy of 2.5 GeV and an undulator that is modeled for the maximum available energy of 14.3 GeV (dedicated undulator):

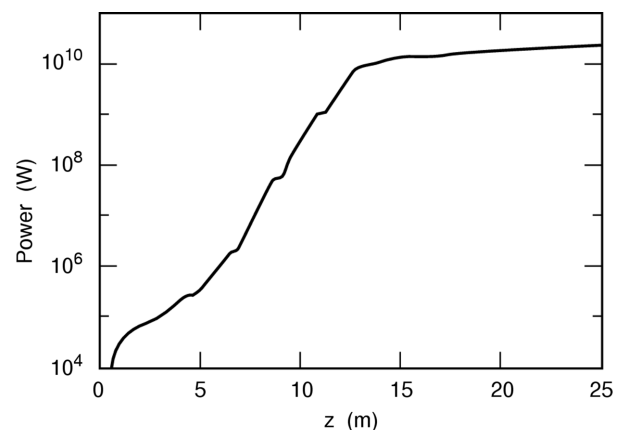


Figure 10 Evolution of the radiation power along the undulator at a wavelength of 50 Å. The FEL saturates in less than 15 m.

(i) The FEL power, peak brightness and photon flux are a factor of ~ 10 higher with a dedicated undulator.

(ii) The saturation length of a dedicated undulator is 70 m, against the 15 m of the baseline undulator.

3.4. Operation at shorter wavelengths

The baseline LCLS operates at a maximum energy of 14.5 GeV, which is the full energy of the presently available last third of the SLAC linac, but only about one-third of its total capacity. The baseline design of the LCLS undulator does not allow the use of energies much higher than 20 GeV owing to the degradation of the electron beam caused by quantum excitation of the spontaneous radiation. Because the emission of these photons is random, it leads to an increased momentum spread in the electron beam that hampers the development of the FEL process. The growth in the variance of the energy spread is given by (Saldin *et al.*, 1996)

$$\Delta(\gamma^2)/dz = (14/30\pi)\lambda_c r_e \gamma^4 k_u^3 a_u^2 F(a_u), \quad (7)$$

where λ_c is the Compton wavelength, r_e is the classical electron radius, k_u is the undulator wavenumber ($2\pi/\lambda_u$, where λ_u is the undulator period length) and a_u is the undulator parameter. The function $F(a_u)$ depends on the undulator type with

$$F(a_u) = 1.42a_u + \frac{1}{1 + 1.50a_u + 0.95a_u^2} \quad (8)$$

for a helical undulator or

$$F(a_u) = 1.70a_u + \frac{1}{1 + 1.88a_u + 0.88a_u^2} \quad (9)$$

for a planar undulator. Fig. 12 shows the FEL amplification for different beam energies and for the baseline LCLS undulator design. The growth in energy spread owing to the quantum excitation of the spontaneous radiation strongly suppresses the FEL amplification at energies higher than ~ 20 GeV.

One way of offsetting the effect of quantum excitation, which is cumulative during the FEL power built-up along the undulator, is to

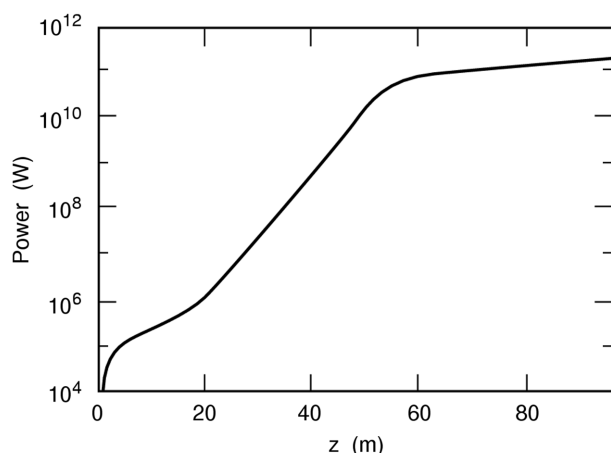


Figure 11 Profile of the FEL power along the undulator length with an 8 cm-long undulator period. The electron energy is 14.3 GeV.

Table 3

Some parameters and performance comparison between the LCLS baseline undulator and a dedicated undulator.

Both generate 50 Å FEL radiation.

	Baseline undulator	Dedicated undulator	Units
Undulator period	3	8	cm
Electron energy	2.48	14.33	GeV
Gap between magnetic poles	1.2	2.0	cm
Peak magnetic field	1.32	1.87	T
Undulator parameter, K	3.7	13.9	
Normalized r.m.s. emittance	2.0	2.0	mm mrad
Peak electron current	3400	3400	A
FEL power at saturation	12	100	GW
Saturation length	15	70	m
Peak photon flux	3×10^{26}	2.6×10^{27}	photons s^{-1}
Coherent photons per pulse	6.9×10^{13}	3.0×10^{14}	photons pulse $^{-1}$
Peak brightness	2.3×10^{31}	2.0×10^{32}	photons $s^{-1} mm^{-2} mrad^{-2}$ (0.1% bandwidth) $^{-1}$

reduce the gain length of the free-electron laser, thus strengthening the lasing action. The maximum saturation length below which the quantum excitation is not important is approximately given by the formula

$$L_{\text{eff}} = [\gamma^2 \lambda_u^2 / (d\Delta\gamma^2/dz)]^{1/3}. \quad (10)$$

Equation (10) is obtained by requiring that the energy spread growth owing to quantum excitation at saturation be equal to the FEL parameter (Bonifacio *et al.*, 1984). For a 50 GeV beam, equation (10) gives $L_{\text{eff}} = 55$ m, a requirement that is not met by the baseline LCLS design, therefore making it unsuitable for operation above ~ 20 GeV. In order to accommodate a higher electron energy beam, thus shorter photon wavelengths, ways must be found to reduce the saturation length. This goal can be achieved by (i) improving the electron beam quality, and/or (ii) a suitable re-design of the undulator. The beam quality can be improved either by a lower emittance or a higher peak current, whichever is easier to achieve. Assuming a normalized emittance of 0.1 mm mrad and a current of 5 kA, a 50 GeV electron beam saturates within 45 m for a helical undulator with an undulator parameter of 2.6 and a period of 3 cm (Fig. 13). A helical undulator has a shorter saturation length than a planar undulator, all other parameters being equal. This design would also have the advantage of not requiring quadrupoles to focus the beam. The benefit of eliminating the quadrupole alignment would be very important. Fig. 13

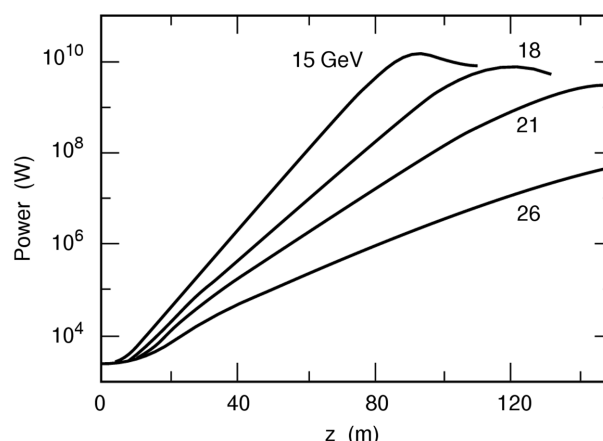


Figure 12 FEL power along the baseline LCLS undulator at electron energies higher than the baseline LCLS. The photon energies follow equation (6).

shows the FEL performance for various lengths of the undulator period. The quantum fluctuations have an effect on the FEL gain for the chosen emittance value of 0.1 mm mrad, a peak current of 5 kA and a period length of 3 cm. When the period length is increased to 4 cm the effect of quantum fluctuations becomes negligible, the saturation length shortens, and the saturation power increases. For period lengths >4 cm, increasing the period length increases the saturation length. Table 4 provides more information about the cases depicted in Fig. 13.

Although the emittance assumed in the calculations and in Fig. 13 (0.1 mm mrad) appears optimistic (the LCLS baseline design value is 1.2 mm mrad), consideration should be given to the long projected time span for the developments discussed in this report. Given sufficient R&D support, and based on past advancements, it is not unreasonable to imagine that electron beam quality improvements of the type envisaged in this report will actually be achieved within the first ten years of LCLS operation, perhaps with an entirely new gun design. The electron beam quality discussed above leaves unused more than half of the entire LCLS space available for the undulator in the baseline design. This fact can be used to advantage by changing the undulator parameters in such a way as to reduce the impact of the quantum fluctuations by reducing the undulator parameter a_u , by

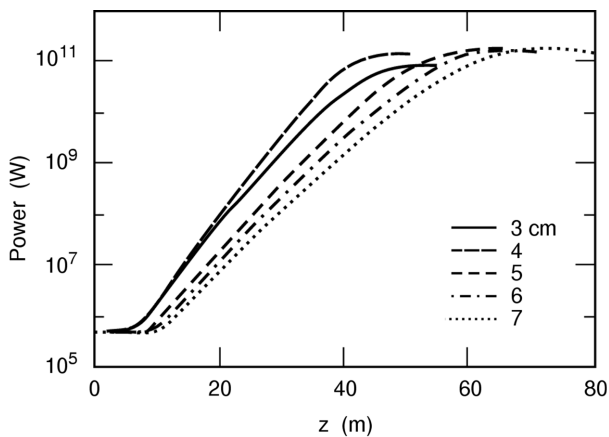


Figure 13
Evolution of the FEL radiation power in a helical undulator with an undulator parameter equal to 2.6 and varying undulator period lengths (3, 4, 5, 6 and 7 cm).

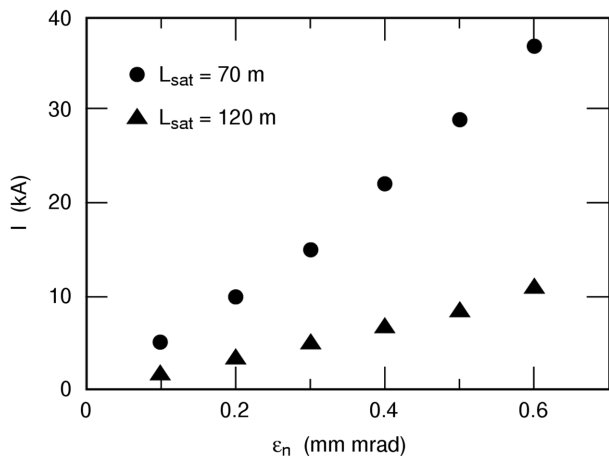


Figure 14
Trade-offs between emittance and peak current for two fixed saturation lengths and FEL powers.

Table 4
Undulator period λ_u , radiation wavelength λ_r , undulator parameter a_u , electron energy E and undulator field B_u for the graphs shown in Fig. 13.

λ_u (cm)	λ_r (Å)	a_u	E (GeV)	B_u (T)
3	0.12	2.6	50	0.93
4	0.16	2.6	50	0.70
5	0.20	2.6	50	0.56
6	0.24	2.6	50	0.46
7	0.28	2.6	50	0.40

increasing the undulator period [as indicated in equation (7)] or both. Increasing the undulator period is preferable since this does not reduce the FEL power output. An additional benefit is that a longer period length results in a larger undulator gap when the undulator parameter is held constant. The effect of undulator wake fields is reduced and it allows a larger aperture for the electron beam transport. Fig. 14 shows the dependence of the maximum electron emittance and minimum peak current needed to reach saturation while keeping the saturation length the same at two different wavelengths. The results for two different saturation lengths in Fig. 14 were obtained; in the 70 m case with a period length of 3 cm and a radiation wavelength of 0.12 Å; and in the 120 m case with a 7 cm period and a radiation wavelength of 0.28 Å.

A longer undulator period would lower the demands on the beam parameters, but increase the radiation wavelength of the FEL. For an undulator like the baseline LCLS design (with an undulator period of 3 cm) the radiation wavelength at an electron energy of 50 GeV is about 0.12 Å, which is a factor of 12 shorter than for the current LCLS design. If the undulator period was lengthened to 7 cm, the required emittance would be relaxed from 0.1 to 0.3 mm mrad, but the radiation wavelength would be increased to 0.28 Å (as in Table 4). This set of parameters would still give a five-times-shorter wavelength than the baseline LCLS and it would utilize the full 50 GeV capacity of the linear accelerator. This is a feasible scenario: the highest beam energy delivered by the linac for experiment E158 in 2002 was 48.75 GeV with a charge of up to 4.5×10^{11} electrons per pulse over a pulse length of ~ 280 ns. These parameters have been achieved routinely for several weeks at a time. The electron energy of 48.75 GeV meets the experimental requirements and was not set by the maximum linac energy. Nevertheless, at this high charge, beam loading becomes significant, but with a pulse of only 6.2×10^9 electrons, as in the baseline LCLS in the single-bunch mode, 50 GeV is achievable with the desired beam characteristics. For multibunch operation, some compromise on the maximum number of bunches that could be accelerated to 50 GeV will need to be made.

4. Utilization of spontaneous radiation in the LCLS

The spontaneous radiation from the baseline LCLS undulator has a larger spectral range and potential for shorter pulse duration than the FEL radiation. These could provide useful experimental opportunities, particularly before the full potential of the LCLS to produce femtosecond FEL pulses is reached. It was discussed in §3 that the LCLS linac is able to run at an energy as low as 2.5 GeV, thus generating coherent light down to 250 eV. In the long-range future, the energy available from the entire length of the SLAC linac, up to 50 GeV, could be used to produce coherent light up to almost 100 keV in the first harmonic. Bunch-shortening techniques on the horizon promise to yield LCLS bunch lengths of ~ 1 fs or shorter. Even with this potential of expansion of the LCLS, there are characteristics in the spontaneous radiation that will make it attractive for

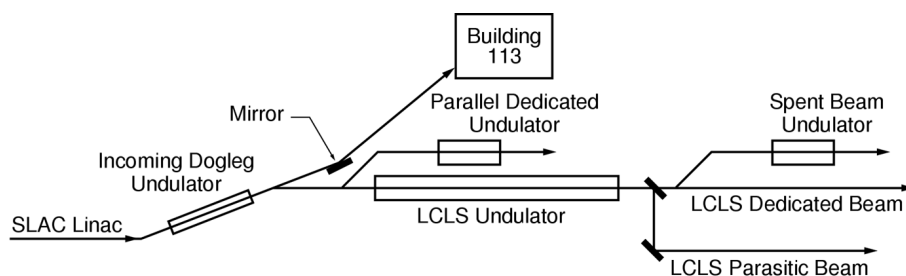


Figure 15
Schematic layout of the five possible strategies for spontaneous radiation.

some experiments. These are the broad band of the spectrum, extending to several hundred keV, and the possibility of shortening the electron bunch in a way that would not be allowed by FEL operation because of its stricter demand on the beam quality. Unlike the SASE amplified noise, the spontaneous radiation provides smooth and reproducible pulses. In some modes of operation, spontaneous radiation could be used with FEL radiation to carry out pump–probe experiments with precise intervals between the sources. Spontaneous radiation, particularly from a tapered undulator, could have broad enough peaks to use for spectroscopy, unlike the FEL.

There are at least five possible sources of spontaneous radiation associated with the LCLS; ‘LCLS parasitic’, ‘LCLS dedicated’, ‘parallel dedicated’, ‘spent beam parasitic’ and ‘incoming dog-leg’ source modes. Fig. 15 illustrates these options.

This section will conclude with a discussion on the possibility of using the spent electron beam from the FEL as a source of THz radiation and as a source of positrons.

4.1. Evaluation of the spontaneous sources

The simplest way to obtain spontaneous radiation from the LCLS is to strip off the spontaneous radiation that surrounds the FEL beam in normal FEL operation. This radiation has about ten times more power than the FEL beam, but is spread out into an undulator spectrum that is weaker than the FEL radiation up to about the seventh harmonic. This is the LCLS parasitic mode. It would offer the possibility of providing a beam to a pump–probe experiment with the LCLS that has a precise known time interval between the two sources. More power and a shorter pulse could be obtained by using the LCLS for dedicated spontaneous radiation production. With no constraints on emittance for FEL operation, a larger current and more bunch compression could be used, but this would compete with FEL operation for beam time.

If dedicated spontaneous beam time were available, a dog-leg upstream from the LCLS could be built to provide beam to a parallel dedicated undulator, which could be circularly polarized, or have a variable minigap. The dog-leg could provide further compression if the beam were energy-chirped. A dog-leg downstream from the LCLS would allow the use of the spent beam from the FEL in a spontaneous radiation undulator, and this beam could be further compressed, as in the dedicated parallel mode. This undulator could also be a novel type, and its radiation could be used in pump–probe experiments with the LCLS beam; the interval between the two sources could be made very precise, as with the parasitic source described above.

None of these four alternatives offers significant advantages over the LCLS in FEL mode in the long run, and it is now foreseen that the LCLS will achieve much shorter pulses than the baseline design in the near future. The LCLS may also be run over a much lower and higher

energy range than the baseline design in the near future. It could be run at 2.5 GeV (for a 250 eV fundamental) from the start-up. It is unlikely that the dedicated modes could compete with the FEL running for LCLS beam time, or for LCLS beamline construction funds. The fifth alternative, ‘incoming dog-leg undulator’ is the one we regard as most favorable. It is possible to place an undulator as long as 12 m in the non-dispersive dog-leg that feeds beam into the FEL undulator (see Fig. 15). It contributes negligible emittance growth, and has an

energy growth of less than 4×10^{-5} . With a 1.75° deflecting mirror, this beam could be steered into the existing SPPS end-station in building 113. The deflecting mirror would allow a safety beam stop to be placed in line with the electron beam, but would allow the photon beam to pass into the end-station. A beam from this device could be run in pump–probe mode with the LCLS, and this undulator could be circularly polarizing, or have a variable minigap. A possible design for a helical undulator that has acceptable energy spread growth and is capable of delivering a 250 eV fundamental peak would be 12 m long with 10.82 cm-long period, $K = 11.94$ and 111 periods, for a nominal first harmonic relative peak width of 9 eV at 1 keV. If this is too narrow for spectroscopy, a tapered undulator could be used to widen this peak, or the gap could be tuned over the desired energy range. This device would be optimized for spectroscopy, so it would be complementary to the FEL, which is optimized for diffraction-type experiments. The output of such an undulator is given in Fig. 16, assuming $\beta_x = \beta_y = 25$ m, $\epsilon_x = \epsilon_y = 0.0427$ nm rad (corresponding to 1.2 mm mrad normalized emittance). The opening half-angle for the first harmonic is 20 μ rad.

4.2. Spent beam as an ultrashort pulse source of electric and magnetic fields

Another possible way of using the spent beam is as an ultrashort electric and magnetic field pulse source, just by putting samples in or near the electron beam itself. An isochronous dog-leg downstream from the LCLS could compress a chirped LCLS bunch to about 15 fs, and this would represent a unique way of generating fast electric and magnetic field pulses. The magnetic field near the electron beam is $B = \mu_0 I / 2\pi r$. For a 50 kA beam the field is 10 T at $r = 1$ mm from the beam, and 100 T at 100 μ m. The peak electric field from an extended bunch of charge is $E = Q / (4\pi\epsilon_0\sigma r)$. For $Q = 1$ nC, a 14.35 GeV electron beam, $\sigma = 20$ μ m long and at $r = 10$ mm, the field is 45 MV m^{-1} , and correspondingly higher nearer the beam. Fields of this magnitude are almost unattainable from any other source, particularly with such short durations. These wake fields are sometimes called terahertz radiation, because 1 ps corresponds to a 1 THz signal. A 10 fs pulse would have components up to 100 THz.

In the field of magnetic research, Hans Siegmann and co-workers have for some years performed very elegant experiments on the fast switching behavior of magnetic materials by allowing fast electron pulses from the final focus test beam at SLAC to pass through magnetic thin films (Back *et al.*, 1999). The resulting magnetization caused by the passage of the electron bunch can be read out by photoelectron microscopy.

Keith Nelson proposes to examine the nonlinear switching behavior of ferroelectric materials, using the high transient electric fields (Nelson, 2003). One can imagine other experiments involving fast

Table 5

Comparison of some operating parameters of the SLAC linac between those achieved by the fixed target program and those of the LCLS in the multibunch mode.

	E158 actual	LCLS baseline design	LCLS multibunch desired
Electron energy (GeV)	48	14.5	14.5
Shortest photon wavelength (Å)	–	1.5	1.5
Repetition rate (Hz)	30	120	120
RF pulse length (ns)	280	280	280
Number of electron bunches per RF pulse	~1000	1	2–60
Electrons per bunch	3.1×10^8	6.2×10^9	6.2×10^9
Electrons per macropulse	2.5×10^{11}	6.2×10^9	1.2×10^{10} – 3.7×10^{11}

field pulses, such as investigations of the Zeeman (magnetic) and Stark (electric) effects in this short-pulse regime.

Conventional THz sources like an Auston switch can provide fields of the order of 1 MV m^{-1} (compared with 45 MV m^{-1}), and they produce radiation mostly in the very low THz frequencies. THz research is rising very fast as a new branch of science, and is likely to be quite important in the future. A THz beamline on the LCLS spent beam would cost much less than an undulator beamline, because it would only require the dog-leg and a beam dump.

4.3. LCLS spent beam as a source of ultrashort positron pulses

If a 1 nC LCLS spent-beam pulse at 14.3 GeV were allowed to strike a W or W-Re target (the optimum length of the target is about 2 cm), it would yield about 29 nC of positrons, and copious bremsstrahlung. The positrons would be prompt, so they would come in a pulse not much longer than the electron pulse, and they would come out in a distribution about 1 rad wide (Sheppard, 2003). Experiments into effects like positron channeling might possibly exploit such a source. Fig. 17 shows a spectrum of the positrons (Sheppard, 2003) created in the target.

5. Pulse structure

The LCLS, in its baseline design, envisages the acceleration and lasing of a single electron bunch at the repetition rate of 120 Hz. The SLAC linac has the capability of accelerating several bunches in a radio-frequency pulse that is 280 ns long (henceforth referred to as the ‘macropulse’). It will be shown in this section that this capability offers the possibility of increasing the number of bunches in a macropulse, and, correspondingly, the FEL X-ray pulses, from 1 to a maximum of 60, with a corresponding increase in average flux and brightness.

5.1. SLAC linac operation in multibunch mode

The requirements of each bunch in the macropulse are the same as those of the baseline design: a charge of 1 nC with a transverse emittance of 1.2 mm mrad. It is useful to recall the performance already delivered by the SLAC linac in the multibunch operation mode for the ‘E158 fixed-target experiment’. Some of its operating parameters are shown and compared with those desired by the LCLS in the multibunch mode in Table 5.

The characteristics that are relevant to multibunch operation are (i) repetition rate; (ii) RF macropulse length; (iii) energy flatness; (iv) versatility of switching energy on a macropulse-to-macropulse basis; (v) versatility in bunch timing; (vi) photoinjector.

5.1.1. Repetition rate. The 120 Hz repetition rate of the SLAC linac is determined by the maximum rate of the RF modulators and cannot

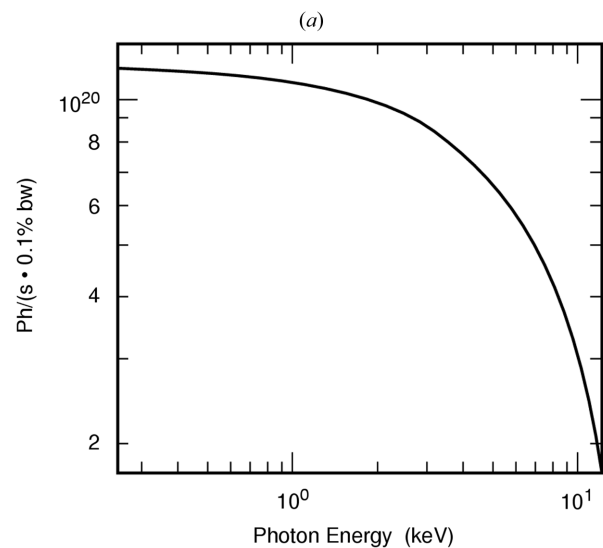
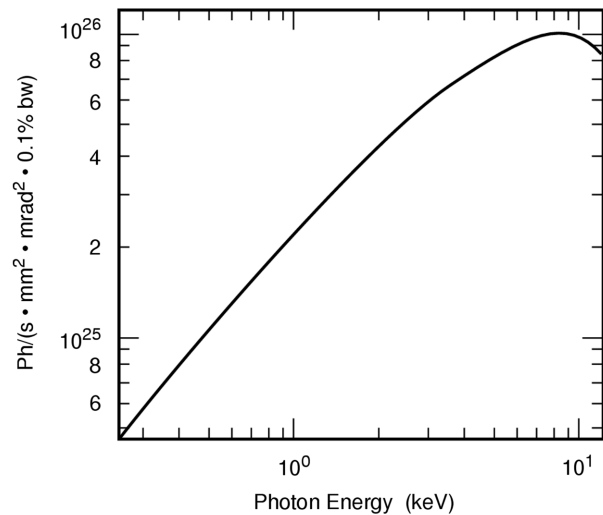


Figure 16 Peak-brightness [in photons $\text{s}^{-1} \text{mm}^{-2} \text{mrad}^{-2} (0.1\% \text{ bandwidth})^{-1}$] and peak-flux [photons $\text{s}^{-1} (0.1\% \text{ bandwidth})^{-1}$] curves for a 12 m helical undulator with parameters given above, based on a peak electron current of 3500 A.

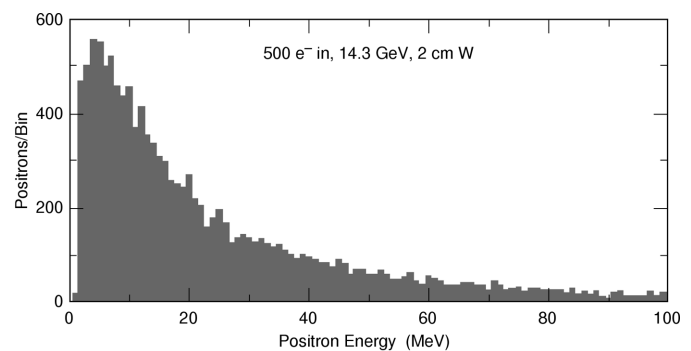


Figure 17 Distribution of the number of positrons created by 500 electrons hitting a target.

be increased without a major and expensive overhaul of the pulse power system.

5.1.2. RF macropulse length. The RF macropulse length of 280 ns is dictated by the SLED process (Decker *et al.*, 1999) and cannot be

Table 6

Time-averaged performance of the LCLS, in single and multibunch modes, and the TESLA XFEL.

	Shortest wavelength (Å)	Repetition rate (Hz)	Number of bunches per macropulse	Average brightness [photons s ⁻¹ mm ⁻² mrad ⁻² (0.1% bandwidth) ⁻¹]	Average flux (photons s ⁻¹)
LCLS baseline	1.5	120	1	2.7×10^{22}	1.2×10^{14}
LCLS multibunch	1.5	120	60	1.6×10^{24}	7.2×10^{15}
TESLA XFEL	1	10	4000	1.6×10^{25}	3.6×10^{16}

increased without a reduction of the accelerating field and, hence, the maximum energy. If one suppresses the field enhancement created by the SLED technique, the RF pulse could be lengthened to 3 μ s, but the maximum energy of the LCLS linac would only be 10 GeV. This appears to be a stiff price to pay and this option is not considered attractive, unless the entire linac becomes available by the time the 3 μ s-long pulse is seriously considered.

5.1.3. Energy flatness. The correlated r.m.s. energy spread of the baseline LCLS design is 0.1% and the multibunch operation should not appreciably increase the spread from bunch to bunch beyond this value in order to avoid an increase of the FEL bandwidth. The factors that determine the uniformity of the energy profile in the longitudinal direction of the bunch are the temporal profile of the electron energy and the beam-loading compensation. When a train of bunches interacts with the accelerating structure, the beam-induced voltage must be compensated in amplitude and phase. A computer simulation (performed by F. J. Decker) of beam loading and its compensation was successfully tested against the measured data of the E158 experiment. These fixed-target experiments require the highest possible electron current. The simulation of a case where the beam loading was 8.5% (at 48.6 GeV), a beam pulse of about 280 ns length and 3.75×10^{11} particles gave a flat energy within 0.1%, in excellent agreement with the experimental results, where the measured energy spread was just 0.1%. Since the LCLS will use 6.2×10^9 particles per bunch, up to ~ 60 bunches in a train could be accelerated ($3.7 \times 10^{11}/6.2 \times 10^9$) for the same beam loading as in the E158 experiment. In this experiment the transient beam loading was compensated by changing the charge per bunch linearly along the macropulse (with 22% of the central charge in the front and 22% in the back). In the LCLS the charge per bunch cannot be varied along the macropulse, since the bunch compression process requires a charge tolerance per bunch of 2% r.m.s. (LCLS, 2002). It is proposed, instead, to change the distance between consecutive bunches. The required change of beam-induced voltage between the head and the tail of the macropulse can be obtained by having the appropriate bunch separation from the front to the back. Although it may be possible to compensate the transient beam loading with a number of bunches that is greater than 60, for the purpose of this report this number, scaled from experimental data, is assumed.

5.1.4. Transverse long-range wake fields and beam break-up. With a charge as high as 9×10^{11} electrons per macropulse, beam break-up was observed in the SLAC linac, attributed to the fact that the transverse dipole mode frequency of 4140 MHz was excited when the bunch separation was 16 RF buckets. A varying bunch separation will decohere this effect and alleviate this problem. Nevertheless, the long-range wake field is of some concern and further study is needed.

5.1.5. Versatility of switching energy on a macropulse-to-macropulse basis. The possibility exists of feeding several undulators at the repetition rate given by $120/N$ Hz, N being the number of undulators. It will be possible to vary the electron energy on a macropulse-to-

macropulse basis, allowing different FEL wavelengths to be shared among different users. The maximum relative electron energy that can be changed on a pulse-by-pulse basis (*i.e.* every 8.3 ms) is the energy acceptance of the linac optics. This gives a change in the FEL photon energy in the range 7.5–8.2 keV. It would be possible to vary the linac

transverse optics on a pulse-to-pulse basis with pulsed quadrupoles, a nontrivial but possible task. This would increase the range up to 5 GeV and the photon range available on a pulse-to-pulse basis would be 0.6–8.2 keV. Finally, kickers and by-pass lines could be introduced to extract the electrons at different points in the linac. Two by-pass lines (at 3 and 9 GeV) and a 30 GeV kicker already exist for PEP-II electron and positron injections. It is not possible to change the energy within the 280 ns RF pulse, as the filling time of the accelerating structure is 800 ns.

5.1.6. Photoinjector development for multibunch operation.

In order to operate in the multibunch mode, the photoinjector must have characteristics that are different, in some respects, from those of the single bunch of the baseline design. The main new aspects are:

(i) The laser repetition rate increases from a single pulse at 120 Hz to 60 pulse trains, each lasting 280 ns with an average bunch separation of about 6 ns. Pockels cells, with a rise time of ~ 1 ns, can be used as switches. R&D effort will be required to achieve the laser intensity. The difficulties can be alleviated with a cathode material of higher quantum efficiency.

(ii) The RF power dissipation in the multibunch mode will not be significantly different from the single-bunch mode, since the RF pulse length in both cases is of the order of 2 μ s.

(iii) Beam loading in the radio-frequency gun may vary the accelerating field from bunch to bunch in the macropulse, and thus the energy, the charge and the charge density of the electrons extracted from the photocathode. This issue should be investigated as part of the R&D program, but it appears to be manageable, as the load is not severe. Since the gun carries a relativistic beam and its gradient is higher than in the linac, beam-loading compensation based on feed-forward amplitude and phase ramp, and the variable bunch spacing envisaged for the linac compensation scheme described in §5.1.3, should be helpful. Additional flexibility is provided by the possibility of modulating the intensity of the laser pulse to match a possible residual variation of charge from bunch to bunch in a macropulse.

5.2. Multibunch operation

The beam-loading compensation scheme described above will allow the acceleration of up to 60 electron bunches per macropulse. The time-averaged performance of such a device, in terms of its average values, is compared with the baseline LCLS and the proposed TESLA X-ray FEL at DESY and is shown in Table 6.

The multipulse operation raises the issue of damage to material and power deposition. The average FEL radiation power in the multibunch mode is 18.75 W, and the average spontaneous radiation power is 217.5 W. Silicon optics cooled at liquid-nitrogen temperature can tolerate up to 1 kW and therefore heat transfer should not be a problem. The power density represents a challenge for the baseline design and it is expected that much will have been understood and advances will have been made by the time the multibunch option is

implemented. In fact, the baseline LCLS will provide valuable data relevant to the power density issue. In the baseline design, the average power density of the FEL radiation in the first harmonic is about 55 W mm^{-2} ; in the multibunch mode this number rises to 3.3 kW mm^{-2} . One mitigating factor in the proposed multibunch configuration will be the short duration of the macropulse (280 ns). Damage will be reduced because the macropulse duration will not be long enough to reach equilibrium in the optical elements, as this is of the order of $1 \mu\text{s}$.

6. Summary

This report discusses the potential of the Linac Coherent Light Source to enhance its capabilities beyond those of the baseline design and of the initial operation. The projections presented in this paper are compatible with the baseline design and make use of the initial capital investment. The upgrades and enhanced use of the LCLS discussed in this report are summarized as follows:

(i) Pulses of FEL radiation that are much shorter than the baseline design value (230 fs with 10^{12} photons per pulse). Several schemes have been proposed and will be investigated as part of the R&D in the LCLS. A novel scheme was presented that appears capable of delivering subfemtosecond-long FEL pulses with 5×10^9 photons per pulse.

(ii) The output power of the FEL radiation could be increased from 20 (baseline value) to 60 GW by tapering the present undulator. Ultimately, a 200 m tapered undulator with seeded radiation would be able to deliver output power approaching 200 GW.

(iii) The baseline LCLS wavelength range ($1.5\text{--}15 \text{ \AA}$) could be extended to $0.12\text{--}50 \text{ \AA}$.

(iv) The LCLS is a copious source of spontaneous radiation. Such radiation has a larger spectral range and shorter pulse duration than the baseline LCLS, and could provide useful experimental opportunities.

(v) The SLAC linac is capable of sustaining the acceleration of several bunches in a macropulse. A conservative assumption indicates that up to 60 bunches could be accelerated in a pulse, giving a corresponding increase in average flux and brightness compared with the baseline design that utilizes only one pulse per macropulse. The system also offers the opportunity of pump-probe experiments utilizing two FEL pulses in a macropulse.

(vi) Terahertz radiation is produced from the spent beam of the LCLS that could be applied to a growing field of research.

(vii) Positron pulses as short as the electron pulses could be generated by impinging the electron beam on a target.

The authors wish to thank Katerina Ioakimidi for sharing with us her knowledge on the response of a photocathode to a short laser pulse. They also wish to thank Roger Erickson for the information on the operation of the SLAC linac, Roger Miller for his comments and suggestions on transient beam loading in the linear accelerator, and Bob Hettel for useful comments. We thank John Sheppard, who provided the computations of the positron production from the LCLS spent beam, and Jym Clendenin and Dave Dowell, who provided valuable comments and suggestions on photoinjector issues. This research was carried out at the Stanford Linear Accelerator Center, a national user facility operated by Stanford University on behalf of the US Department of Energy, and was supported by the DOE Office of Science.

References

- Back, C. H., Allenspach, R., Weber, W., Parkin, S. S. P., Weller, D., Garwin, E. L. & Siegmann, H. C. (1999). *Science*, **285**, 864–867.
- Bharadwaj, V. V., Chao, A., Cornacchia, M., Emma, P., Kotseroglou, T., Krejcik, P., Lindau, I., Nuhn, H.-D., Stupakov, G., Tatchyn, R., Bionta, R., Toor, A. & Pellegrini, C. (2000). SLAC-LCLS Report LCLS-TN-00-8. Stanford Linear Accelerator Center, Stanford, CA, USA.
- Bonifacio, R., Pellegrini, C. & Narducci, L. (1984). *Opt. Commun.* **50**, 373–378.
- Borland, M. D., Chae, Y.-C., Lewellen, J. W., Milton, S. V., Soliday, R., Bharadwaj, V., Emma, P., Krejcik, P., Nuhn, H.-D. & Fawley, W. M. (2002). *Nucl. Instrum. Methods*, **A483**, 268–272.
- Decker, F. J., Farkas, Z. D. & Turner, J. (1999). *Proceedings of the 1999 Particle Accelerator Conference*, <http://epaper.kek.jp/p99/procs.htm>.
- Emma, P., Bane, K., Cornacchia, M., Huang, Z., Schlarb, H., Stupakov, G. & Walz, D. (2004). *Phys. Rev. Lett.* **92**, 074801-4.
- Fawley, W., Huang, Z., Kim, K.-J. & Vinokurov, N. (2002). *Nucl. Instrum. Methods*, **A483**, 537–541.
- Kim, K.-J. (1986). *Phys. Rev. Lett.* **57**, 1871–1874.
- LCLS (2002). Conceptual Design Report SLAC-R-593. Stanford Linear Accelerator Center, Stanford, CA, USA.
- Moore, G. T. (1985). *Nucl. Instrum. Methods*, **A239**, 19–28.
- Nelson, K. (2003). Private communication.
- Reiche, S., Pellegrini, C., Rosenzweig, J. B., Emma, P. & Krejcik, S. (2002). *Nucl. Instrum. Methods*, **A483**, 70–74.
- Saldin, E. L., Schneidmiller, E. A. & Yurkov, M. V. (1996). *Nucl. Instrum. Methods*, **A381**, 545–547.
- Scharlemann, E. T. (1990). *Laser Handbook*, edited by W. B. Colson, C. Pellegrini and A. Renieri, p. 314. Amsterdam: North Holland.
- Scharlemann, E. T., Sessler, A. M. & Wurtele, J. S. (1985). *Phys. Rev. Lett.* **54**, 1925–1928.
- Sheppard, J. (2003). Private communication.
- Xie, M. (2000). *Nucl. Instrum. Methods*, **A250**, 59–66.
- Xie, M. & Deacon, D. A. G. (1986). *Nucl. Instrum. Methods*, **A250**, 426–431.
- Wang, J.-M. & Yu, L.-H. (1986). *Nucl. Instrum. Methods*, **A250**, 484–489.
- Yu, L.-H., Krinsky, S. & Gluckstern, R. (1990). *Phys. Rev. Lett.* **50**, 3011.